NASA
Technical
Paper
2500

August 1985

# Mechanics of a Gaseous Film Barrier to Lubricant Wetting of Elastohydrodynamically Lubricated Conjunctions

Joseph M. Prahl and
Bernard J. Hamrock



NASA

**NASA Technical Paper 2500**

1985

# Mechanics of a Gaseous Film Barrier to Lubricant Wetting of Elastohydrodynamically Lubricated Conjunctions

Joseph M. Prahl
*Case Western Reserve University*
*Cleveland, Ohio*

Bernard J. Hamrock
*Lewis Research Center*
*Cleveland, Ohio*

National Aeronautics and Space Administration

**Scientific and Technical Information Branch**

## Summary

Two analytical models, one based on simple hydrodynamic lubrication (HL) and the other on elastohydrodynamic lubrication for materials of low elastic modulus (soft EHL) are presented and compared to delineate the dominant physical parameters that govern the mechanics of a gaseous film between a small drop of lubricant and the outer race of a ball bearing. Both models are based on the balance of gravity forces, air drag forces, and air film lubrication forces and incorporate a drag coefficient $C_D$ and a lubrication coefficient $C_L$ to be determined from experiment. The soft EHL model considers the effects of droplet deformation and solid surface geometry, whereas the simpler HL model assumes that the droplet remains essentially spherical. The droplet's angular position depends primarily on the ratio of gas inertia to droplet gravity forces and on the gas Reynolds number and weakly on the ratio of droplet gravity forces to surface tension forces (Bond number) and geometric ratios for the soft EHL.

An experimental configuration in which an oil droplet is supported by an air film on the rotating outer race of a ball bearing within a pressure-controlled chamber produced measurements of droplet angular position as a function of outer-race velocity, droplet size and type, and chamber pressure. For Bond numbers less than 0.5 (larger surface tension forces), both models correlate the experimental data with a nearly constant $C_D$ of 0.4 and a $C_L$ of 3.0 for HL or 1.0 for soft EHL. For larger variations in Bond number $B$ and Reynolds number $\mathrm{Re}_D$, the soft EHL model shows superior correlation of the experimental data with experimentally determined $C_D$ versus $\mathrm{Re}_D$ and $C_L$ versus $B$.

## Introduction

Although the amount of lubricant needed to sufficiently lubricate a nonconformal contact elastohydrodynamically is small, a critical amount is needed to maintain a fully flooded conjunction. Nonconformal contacts are normally found in mating gear teeth, cams and followers, and rolling-element bearings. If the amount of fluid in the conjunction goes below the critical amount, the conjunction becomes starved and the minimum film thickness is considerably reduced, as shown by Hamrock and Dowson (1977). If the starvation is continued, the nonconformal contact will eventually fail.

Kingsbury (1969) reported the failure of large lubricant droplets to wet and enter the conjunction of a rolling-element bearing, thereby causing lubricant starvation. Starvation is caused by the presence of a gaseous film barrier between the droplet and the bearing race surface. The present work presents experimental and theoretical results that delineate the physical parameters that govern the behavior of a stable droplet on a gas film.

The experimental apparatus consisted of an outer race of a ball bearing rotating in the presence of air within a pressure chamber while the equilibrium position of various liquid droplets was measured. The droplet position was recorded as the angle subtended by the radial line from the center of rotation to the droplet center and the vertical line through the rotational center, for the range 20° to 70°.

The physical parameters and their ranges were

(1) Droplet radius, 1 to 1.75 mm
(2) Velocity of the outer race, 2 to 10 m/s
(3) Chamber pressures, 98.6, 68.9, and 34.5 kPa
(4) Three lubricating oils

Besides accurately measuring the position of the droplet for these parameters, an analytical model was developed that describes the position of the droplet as a function of the forces acting on it. The forces considered were gravity, drag, skin friction, and lubrication. Two approaches to quantifying the lubrication force were considered and compared: a semiempirical hydrodynamic model (HL) that assumes the droplet shape to be essentially spherical, and an elastohydrodynamic model for materials of low elastic modulus (soft EHL), which accounts for droplet deformation. By weighing the relative importance of the physical parameters in the problem, the effects of surface tension, gravity, air density, and air viscosity were delineated through the dimensionless ratios of the Reynolds and Bond numbers and the ratio of air inertia to oil gravity forces (a modified Froude number). The predictions of the droplet angular position versus modified Froude, Bond, and Reynolds numbers were compared for the two models. These results were compared with the experimental measurements taken over a wide range of operating parameters.

We wish to thank Dr. E.P. Kingsbury of Charles S. Draper Laboratory for bringing this problem to our attention and for contributing elements of the experimental apparatus.

## Symbols

| | |
|---|---|
| $B$ | Bond number, $\rho_{oil} r_d^2 g/\sigma$ |
| $C_D$ | drag coefficient |
| $C_{EHL}$ | elastohydrodynamic lubrication coefficient |
| $C_L$ | $C_{L,2}/(C_{L,1})^{1/2}$ |
| $C_{L,1}$ | hydrodynamic lubrication coefficient |
| $C_{L,2}$ | skin friction coefficient |
| $D_x$ | diameter of contact ellipse along direction of motion, m |
| $D_y$ | diameter of contact ellipse along transverse direction, m |
| $d_d$ | diameter of droplet, m |
| $E$ | modulus of elasticity, Pa |
| $E'$ | effective modulus of elasticity, $2/[(1-\nu_d^2)/E_d+(1-\nu_d^2)/E_b]$, Pa |
| $\mathcal{E}$ | complete elliptical integral of second kind |
| $F$ | modified Froude number, or EHL lubrication force, N |
| $g$ | gravitational constant, m/s$^2$ |
| $h$ | film thickness, m |
| $h_{min}$ | minimum film thickness, m |
| $k$ | ellipticity parameter, $D_y/D_x$ |
| $P_c$ | chamber pressure, Pa |
| $P_0$ | ambient pressure, Pa |
| $R$ | curvature sum, m |
| $R_c$ | correlation coefficient |
| $Re_D$ | air Reynolds number, $\rho_{air} V d_d/\eta_{air}$ |
| $r$ | radius of curvature, m |
| $r_d$ | radius of oil droplet, m |
| $u$ | surface velocity in direction of motion, $(u_d+V)/2$, m/s |
| $V$ | velocity of outer race, m/s |
| We | Weber number, $\rho_{air} V^2 d_d/\sigma$ |
| $w$ | weight of oil droplet, N |
| $\eta$ | absolute viscosity at gauge pressure, N s/m$^2$ |
| $\theta$ | angular position of droplet |
| $\nu$ | Poisson's ratio |
| $\rho$ | lubricant density, N s$^2$/m$^4$ |
| $\sigma$ | surface tension, N/m |

Subscripts:

| | |
|---|---|
| $b$ | outer race |
| $d$ | oil droplet |
| $x,y$ | coordinate system |
| 0 | ambient conditions |

## Experimental Apparatus

An apparatus was assembled to exhibit the phenomenon of air film droplet suspension on a rotating surface and to make the characteristics of this phenomenon amenable to measurement. The equipment (fig. 1) consisted of the outer race of a ball bearing mounted with its axis of rotation horizontally supported by two ball bearings within a pressure chamber. A removable glass viewing port was placed normal to the axis of rotation and close to the droplet location for ease of droplet insertion. The outer race and shaft assembly were driven by a variable-speed motor drive through an O-ring seal in the chamber opposite the viewing port. The rotational speed of the motor was proportional to the input voltage, measured by a digital voltmeter. A strobescope was used to obtain precise rotational speeds. Suitable couplings were placed between the sealed shaft of the motor and the outer-race shaft assemblage to ensure vibration-free rotation. The three chamber pressures (98.6, 68.9, and 34.5 kPa) were measured by an absolute pressure gauge and were maintained by adjusting a bleed valve to the atmosphere while evacuating the chamber with a vacuum pump.

The droplet's size and angular position on the race were determined with a cathetometer mounted on a horizontal traversing compound. A sectional view of the outer race and a typical droplet location are shown in figure 2.

## Test Procedure

Before each day's tests the cathetometer was leveled and adjusted so that the telescopic site moved in a plane parallel to the plane of rotation of the outer race. The eyepiece scale of the cathetometer was calibrated by placing a steel ball of precisely 0.318 cm (0.125 in) diameter on the outer race and measuring its diameter as a given number of units of the eyepiece scale. The horizontal and vertical readings of the position of the outer-race rotational center were checked frequently so that they, combined with the droplet's horizontal and vertical position, could be used to determine the droplet's angular position $\theta$.

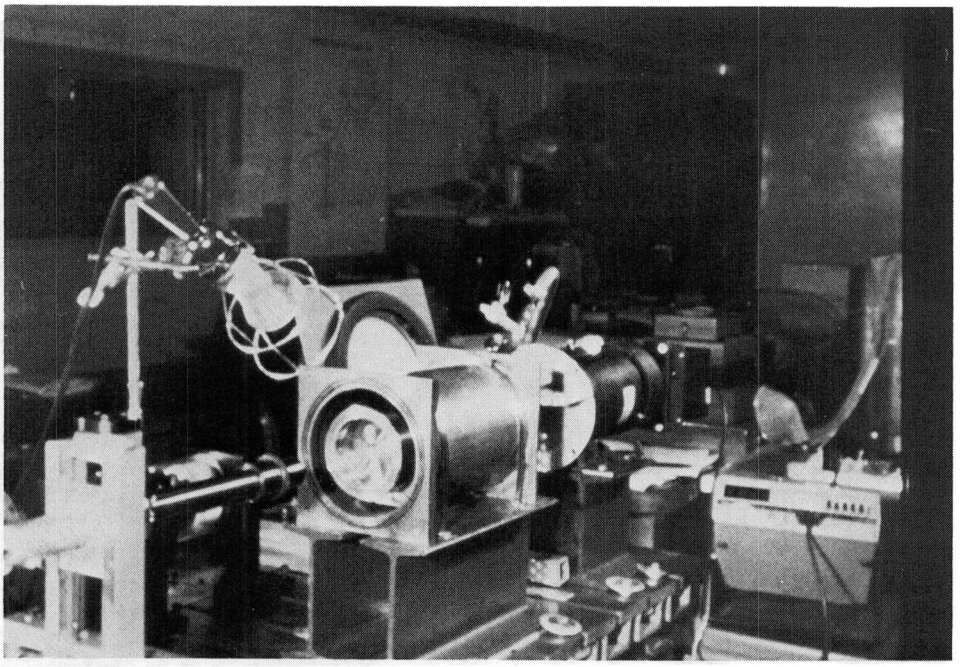

Figure 1.—Experimental apparatus, showing rotating outer race, pressure chamber, drive motor, cathetometer, and traversing compound.

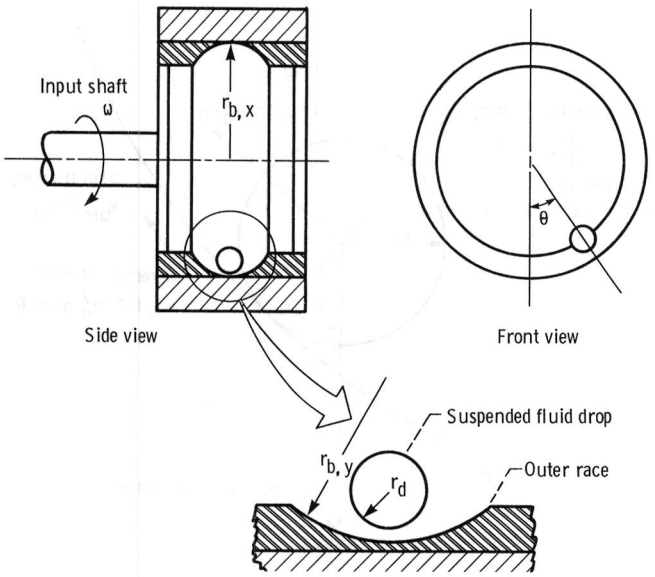


Figure 2.—Sectional view of outer race and drop location.

The ambient pressure in the laboratory was compared with the absolute pressure gauge's reading to ensure proper operation of the gauge. The ambient temperature of the laboratory was checked to ensure that the laboratory's constant-temperature control was functioning.

Once these preliminary steps had been followed, the test oil was drawn into a small syringe, and a droplet was inserted onto the rotating outer race (fig. 3). This was accomplished with the window removed from the chamber and at ambient conditions. Initially the rotational velocity for a stable droplet angular position was not known. After a few trials the approximate velocity range for droplet insertion was determined. The droplet's size could be altered by adding fluid to, or extracting fluid from, a droplet while it was on an air film in the apparatus. Once a droplet of approximately the desired size was situated on the rotating outer race, the glass viewing port was placed on the O-ring and held in place by rubber bands.

The droplet diameter was measured in the tangential and radial directions while the droplet was suspended at a stable position on the rotating race, usually at about 45°. Only for the largest droplets tested was there a measurable difference between the tangential and radial diameters, since the inaccuracy in the measurements of size on the fluctuating droplet was of the same order as the variation in droplet dimensions. The average of the two readings was used throughout the runs on a given droplet, although at angles near 60° the droplet was visibly misshapen by the excessive air inertial forces.

The normal procedure was to work the droplet from the lowest angle (found by trial and error to be about 15°) through to the highest angle for which the droplet appeared stable by increasing the velocity of the race systematically at ambient pressure. At about 60° to 65° the droplet stood off the race and began to oscillate in the axial as well as the tangential direction. The droplet's position was recorded at each rotational velocity, usually in increments of 100 rpm. With the same droplet, if the experimenter had avoided losing the droplet at either end of the angle domain, the pressure was dropped to 68.9 kPa while the velocity of the race was manually

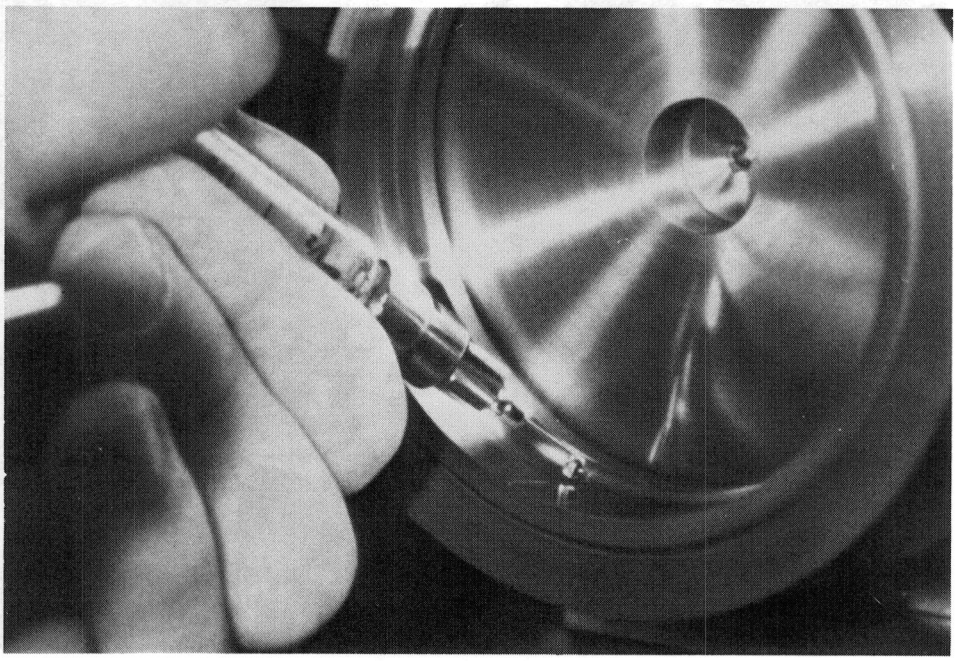

Figure 3.—Droplet insertion onto rotating outer race with hypodermic syringe.

raised to maintain the droplet in the most stable angle range of about 45°. The race velocity was again raised from the lowest "safe" value through to the highest value while angles were recorded and the pressure was checked to ensure constancy. The pressure was then lowered to 34.5 kPa while the droplet's angular position was preserved at 45° by manually raising the race velocity. The reproducibility of this overall procedure for a given droplet was better than 1 to 2 percent and from droplet to droplet was of the order of 5 percent since the most imprecise measurement stems from the droplet size determination.

## Model

A simplified view of a droplet of liquid positioned on the rotating outer race of a ball bearing looking along an axis through the droplet center and parallel to the axis of rotation is sketched in figure 4. The important forces are indicated in the figure. The tangential and radial force balance can be written for a simple hydrodynamic model as

$$\frac{C_D \rho_{\text{air}} V^2 \pi r_d^2}{2} + \frac{C_{L,2} \eta_{\text{air}} V \pi r_d^2}{h} - w \sin\theta = 1 \qquad (1)$$

$$\frac{C_{L,1} \eta_{\text{air}} V \pi r_d^2}{h} \left(\frac{r_d}{h}\right) - w \cos\theta = 0 \qquad (2)$$

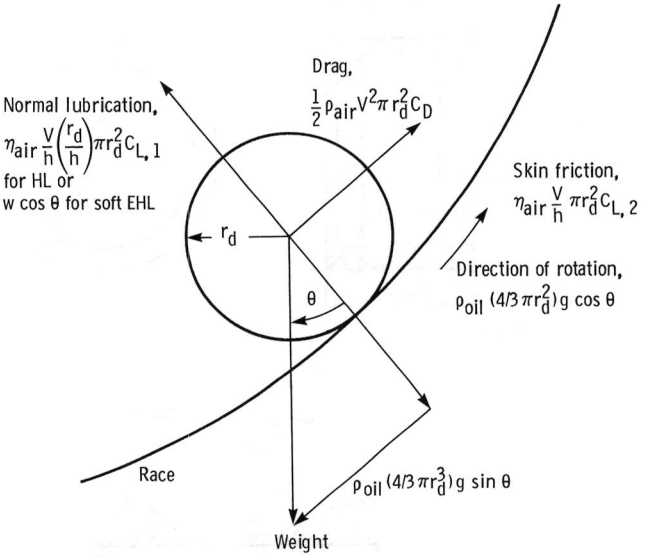


Figure 4.—Schematic of droplet on outer race with characteristic forces of weight, air drag, and air film lubrication.

where $\rho_{\text{air}}$ and $\eta_{\text{air}}$ are the air density and viscosity, respectively, $w$ is the oil droplet weight, $r_d$ is the droplet radius, $h$ is the film thickness, $V$ is the outer-race velocity, $\theta$ is the droplet angular position, $C_D$ is the drag coefficient, and $C_{L,2}$ and $C_{L,1}$ are skin friction and lubrication coefficients, respectively, introduced to absorb geometric considerations not included in this simplified model. The frontal area of the droplet and the droplet contact area are both set to $\pi r_d^2$ with the coefficients $C_D$, $C_{L,1}$, and $C_{L,2}$ expected to correct for the inadequacies of these assumptions.

By combining equations (1) and (2) and rearranging terms, the following relation for predicting $\theta$ was obtained:

$$\sin\theta = \frac{3C_D\rho_{air}V^2}{8\rho_{oil}gr_d} + C_{L,2}\left(\frac{3\eta_{air}V}{4\rho_{oil}gr_d^2}\right)^{1/2}\frac{(\cos\theta)^{1/2}}{(C_{L,1})^{1/2}} \qquad (3)$$

where $\rho_{oil}$ is the oil droplet's density and $g$ is gravity.

In figure 4 the droplet is shown as spherical, implying that the air-oil surface tension forces are large as compared with gravity and air inertia. If in fact the droplet shape deviates appreciably from spherical because surface tension forces are not dominant, a more complex model than that just presented is required to predict $\theta$ as a function of fluid properties, race velocity, and gravity. The elastohydrodynamic theory of Hamrock and Dowson (1978) for materials of low elastic modulus (soft EHL) is an attractive candidate for a model that considers deformation of the droplet in spite of the fact that droplet deformation cannot be precisely characterized as deformation of an elastic solid. The lubrication force in equation (2) therefore is represented by the elastohydrodynamic lubrication model. Furthermore in equation (1) the skin friction term can be more accurately described by defining the contract area of the deformed drop as $\pi D_x D_y/4$ instead of $\pi r_d^2$ as was done in the hydrodynamic model. The tangential and radial force balances that result for the soft EHL model are

$$\frac{C_D\rho_{air}V^2\pi r_d^2}{2} + \frac{C_{EHL}\eta_{air}V\pi D_x D_y}{4h_{min}} - w\sin\theta = 0 \qquad (4)$$

$$E'R_x^2\left[7.43\left(\frac{R_x}{h_{min}}\right)(1-0.85\,e^{-0.31k})\left(\frac{\eta_{air}u}{E'R_x}\right)^{0.65}\right]^{4.76} - w\cos\theta = 0 \qquad (5)$$

where

$$R_x = \frac{r_d r_{b,x}}{r_d + r_{b,x}}$$

$$R_y = \frac{r_d r_{b,y}}{r_d + r_{b,y}}$$

$$u = \frac{u_d + V}{2} = \frac{V}{2}$$

$$E' = \frac{2}{\frac{1-\nu_d^2}{E_d} + \frac{1-\nu_b^2}{E_b}}$$

Following the convention that convex surfaces have positive curvatures and concave surfaces, negative curvatures, the droplet will have a positive radius and the two radii of the outer race will be negative.

Surface tension and gravity affect the droplet shape: the local radii of curvature of the droplet near the contact area must be such that the surface tension forces can support the hydrostatic pressure within the droplet. This internal pressure is characterized as $\rho_{oil}d_d g\cos\theta$, where the droplet height is assumed to be nearly $d_d$. The low modulus of elasticity of the droplet, approximated as the pressure within the droplet resulting from the surface tension forces, is then also equal to $\rho_{oil}d_d g\cos\theta$. Furthermore the modulus of elasticity of the droplet is orders of magnitude less than that of the outer race, and Poisson's ratio of the liquid is assumed to be 0.5. Making use of this, the effective modulus of elasticity becomes

$$E' = \frac{8\rho_{oil}gd_d\cos\theta}{3}$$

From Hamrock and Brewe (1983) simplified equations for the ellipticity parameter and the elliptic integral of the second kind are

$$k = \frac{D_y}{D_x} = \left(\frac{R_y}{R_x}\right)^{2/\pi}$$

$$\varepsilon = 1 + \left(\frac{R_x}{R_y}\right)\left(\frac{\pi-1}{2}\right)$$

These equations can be used to define the elliptical contact diameters in the $x$ direction (direction of motion) and in the $y$ direction (transverse direction), which are expressed in equation (4) as

$$D_x = 2\left(\frac{6\varepsilon wR}{\pi kE'}\right)^{1/3}$$

$$D_y = 2\left(\frac{6k^2\varepsilon wR}{\pi E'}\right)^{1/3}$$

where

$$\frac{1}{R} = \frac{1}{R_x} + \frac{1}{R_y}$$

and

$$w = \rho_{oil}\left(\frac{4\pi r_d^3}{3}\right)g$$

The radial force balance can be simplified and put into a form similar to that of the hydrodynamic model.

$$\left(\frac{\eta_{air} V \pi r_d^2}{h_{min}}\right)\left(\frac{r_d}{h_{min}}\right)^{0.54}\left[\frac{2.96(1-0.85\ e^{-0.31k})^{1.54}}{\left(1+\frac{r_d}{r_{b,x}}\right)^{1.18}}\right] - w\cos\theta = 0 \qquad (6)$$

The soft EHL model includes droplet and outer-race geometry and thus eliminates the need for the empirical coefficient $C_{L,1}$ of the hydrodynamic model. More significantly, the $r_d/h_{min}$ factor magnifying the ratio of normal force to tangential force is to the 0.54 power as compared with the first power in the hydrodynamic model.

By combining equations (4) and (6) and rearranging terms, the following relation for predicting $\theta$ is obtained:

$$\sin\theta = \frac{3C_D\rho_{air}V^2}{8\rho_{oil}gr_d} + C_{EHL}\left(\frac{3\eta_{air}V}{4\rho_{oil}gr_d^2}\right)^{0.35}(\cos\theta)^{0.65} \times \frac{0.4943\left(1+\frac{r_d}{r_{b,x}}\right)^{0.77} D_x D_y}{(1-0.85\ e^{-0.31k})\ 4r_d^2} \qquad (7)$$

Comparing equations (3) and (7) shows the effects of the soft EHL model primarily in the power of the parameter $3\eta_{air}V/4\rho_{oil}gr_d^2$ being 0.35 instead of 0.5 and in the power of the cos $\theta$ term being 0.65 instead of 0.5.

Equations (3) and (7) are both of the form

$$R = f\left\{\frac{\rho_{air}V^2}{\rho_{oil}gr_d}, \frac{\eta_{air}V}{\rho_{oil}gr_d^2}, C_D, C_L, \frac{x_i}{r_d}\right\} \qquad (8)$$

where $x_i/r_d$ represents the length ratios $r_{b,x}/r_d$ and $r_{b,y}/r_d$. The drag coefficient $C_D$ is expected to be a weak function of the air Reynolds number $\rho_{air}Vd_d/\eta_{air}$, which is twice the ratio of the first and second groups in equation (8). The lubrication coefficient $C_L$ might have some dependence on surface tension for large droplets. Comparing gravity forces with surface tension results in the Bond number $\rho_{oil}r_d^2g/\sigma$. Equation (8) can be put in the alternative form

$$\theta = f\left\{F, \mathrm{Re}_D, B, \frac{x_i}{r_d}\right\} \qquad (9)$$

where $F$ is the modified Froude number and $C_D(\mathrm{Re}_D)$ and $C_L(B)$ are relations that we obtain by comparing theory and experiment for a variety of fluids. Note that the product of the first and third groups in equation (9) is 1/2 Weber number, $\rho_{air}V^2d_d/\sigma$, which plays a role in the droplet shape if air inertial forces become excessively large as compared with the surface tension. Dimensionless scalings with the ranges experienced in the tests are presented in table I.

TABLE I.—DIMENSIONLESS SCALINGS

| Dimensionless scalings | Low | High |
|---|---|---|
| $\frac{\text{Air inertia}}{\text{Surface tension}} = \frac{\rho_a V^2/2}{2\sigma/r_d} = \frac{\rho_a V^2 r_d}{4\sigma} = \frac{1}{8}\mathrm{We}_D$ | 0.1 | 1.5 |
| $\frac{\text{Gravity}}{\text{Surface tension}} = \frac{\rho_{oil}2r_dg}{2\sigma/r_d} = \frac{\rho_{oil}gr_d^2}{\sigma} = B$ | 0.3 | 1.4 |
| $\frac{\text{Air inertia}}{\text{Air viscosity}} = \frac{\rho_{air}V^2/2}{\eta_{air}V/r_d} = \frac{\rho_{air}Vd_d}{4\eta_{air}} = \frac{1}{4}\mathrm{Re}_D$ | 50 | 500 |
| $\frac{\text{Air inertia}}{\text{Air film viscosity}} = \frac{\rho_{air}V^2/2}{\eta_{air}V/h} = \frac{\rho_{air}Vh}{2\eta_{air}} = \frac{1}{4}\mathrm{Re}_D\left(\frac{h}{r_d}\right)$ | 1.5 | 40 |
| $\frac{\text{Air film inertia}}{\text{Air film viscosity}} = \frac{\rho_{air}V^2/4r_d}{\eta_{air}V/h^2} = \frac{\rho_{air}Vd_d}{8\eta_{air}}\left(\frac{h}{r_d}\right)^2$ | 0.01 | 0.5 |

## Results

Three oils were tested extensively: synthetic paraffin (XRM 109 F-3), fluorosilicone (XF 10301), and four-ring polyphenyl ether (MCS 210). The relevant properties of these fluids at 25 °C are given in table II.

TABLE II.—FLUID PROPERTIES AT 25 °C

| Fluid | Surface tension, N/m | Density, kg/m³ | Viscosity, kg/m s |
|---|---|---|---|
| Synthetic paraffin (XRM 109 F-3) | 0.0303 | 840 | 0.840 |
| Fluorosilicone (XF 10301) | .0250 | 1150 | .055 |
| Four-ring polyphenyl ether (MCS 210) | .0448 | 1180 | .177 |

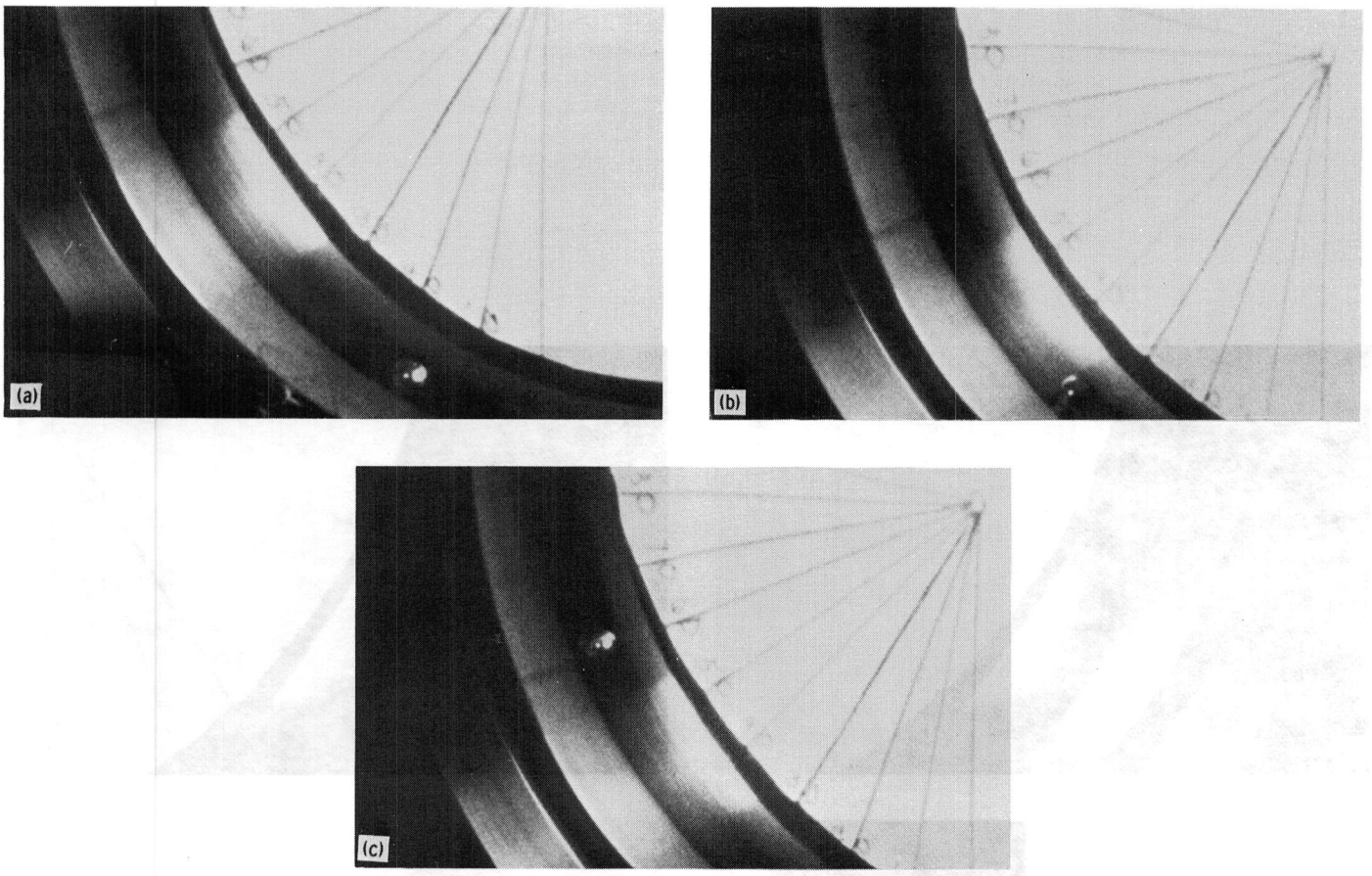


(a) $V = 2.85$ m/s; $We_D = 0.47$; $Re_D = 410$.
(b) $V = 5.30$ m/s; $We_D = 1.6$; $Re_D = 760$.
(c) $V = 7.74$ m/s; $We_D = 3.5$; $Re_D = 1100$.

Figure 5.—Four-ring polyphenyl ether (MCS 210) droplet of 1.08-mm radius in air at Bond number of 0.30 and chamber pressure of 98.6 kPa for varying outer-race velocities and Weber and Reynolds numbers (based on diameter).

The radii of curvature of the outer race are $r_{b,x} = -38.9$ mm and $r_{b,y} = -6.55$ mm, and the rms roughness is approximately 0.5 to 1 $\mu$m in the $y$ direction and 0.1 to 0.2 $\mu$m in the $x$ direction.

Figures 5 and 6 illustrate the characteristics of a 1.08-mm-radius droplet of four-ring polyphenyl ether (MCS 210) at a small Bond number (0.30). The velocity of the outer race was raised from 2.85 to 5.30 to 7.74 m/s at a chamber pressure of 98.6 kPa (fig. 5). The dominance of the surface tension forces gave the droplet a generally spherical appearance. The Weber and Reynolds numbers are given on each figure. The maximum We of 3.5 (fig. 5(c)) occurred at the highest velocity and largest angle, near 60°, but 1/8 We = 0.40, which from table I is most nearly a measure of air inertia to surface tension forces, is still less than unity and the droplet did not appear to deviate substantially from spherical.

Figure 6 shows the effect of reducing the chamber pressure from 98.6 to 68.9 to 34.5 kPa at a substantially constant velocity near 8 to 9 m/s for the same droplet of MCS 210 at a Bond number of 0.30. Since the air density in the chamber was proportional to the chamber pressure, $\theta$ fell from 60° to 50° to about 40° as the pressure was reduced.

Figures 7 and 8 illustrate the alterations in the shape of a 1.98-mm-radius droplet of MCS 210 at a Bond number of 1.0. Raising the outer-race velocity from 5.30 to 7.54 m/s at a chamber pressure of 98.6 kPa (fig. 7) caused the Weber number to vary from 3.0 to 6.1 to 10.0. In figure 7(c), 1/8 We exceeds unity and the shape of the droplet is considerably different from a sphere. Figure 8 again shows the effect of chamber pressure reduction for this large drop of MCS 210 at a fixed outer-race velocity of 9.8 m/s as $\theta$ decreased from 50° to 40° to about 15°.

The results of $\theta$ versus outer-race velocity $V$ for an oil droplet of known physical properties and radius $r_d$ at a given chamber pressure $P_c$ were used in conjunction with the prediction equations (3) and (7) to determine the drag and lubrication coefficients. Equation (3) was put in the form

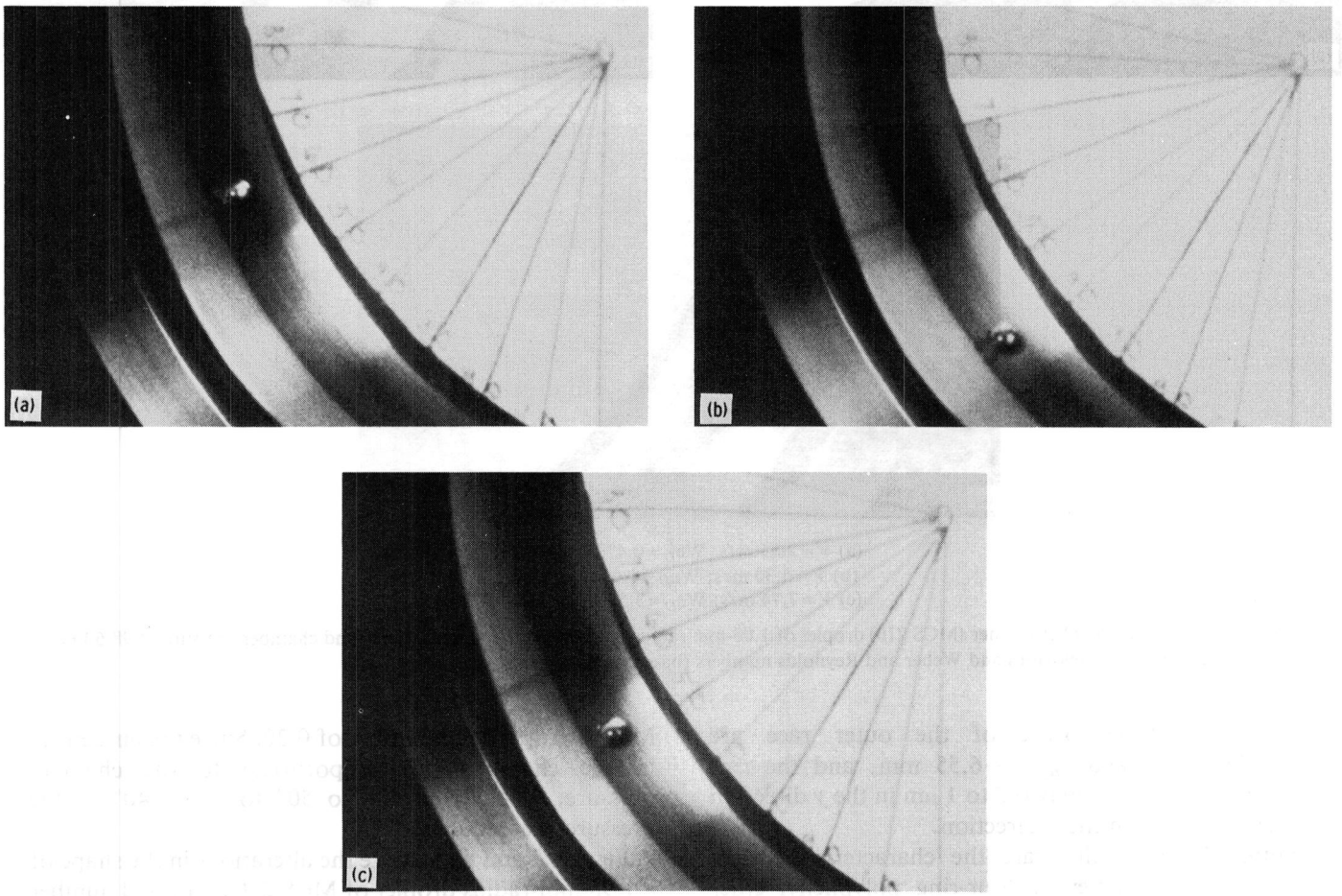


(a) $V = 7.74$ m/s; $We_D = 3.5$; $Re_D = 1100$; $P_c = 98.6$ kPa.
(b) $V = 7.74$ m/s; $We_D = 2.4$; $Re_D = 780$; $P_c = 68.9$ kPa.
(c) $V = 8.96$ m/s; $We_D = 1.6$; $Re_D = 450$; $P_c = 34.5$ kPa.

Figure 6.—Four-ring polyphenyl ether (MCS 210) droplet of 1.08-mm radius in air at Bond number of 0.30 for varying outer-race velocities, Weber and Reynolds numbers (based on diameter), and chamber pressures.

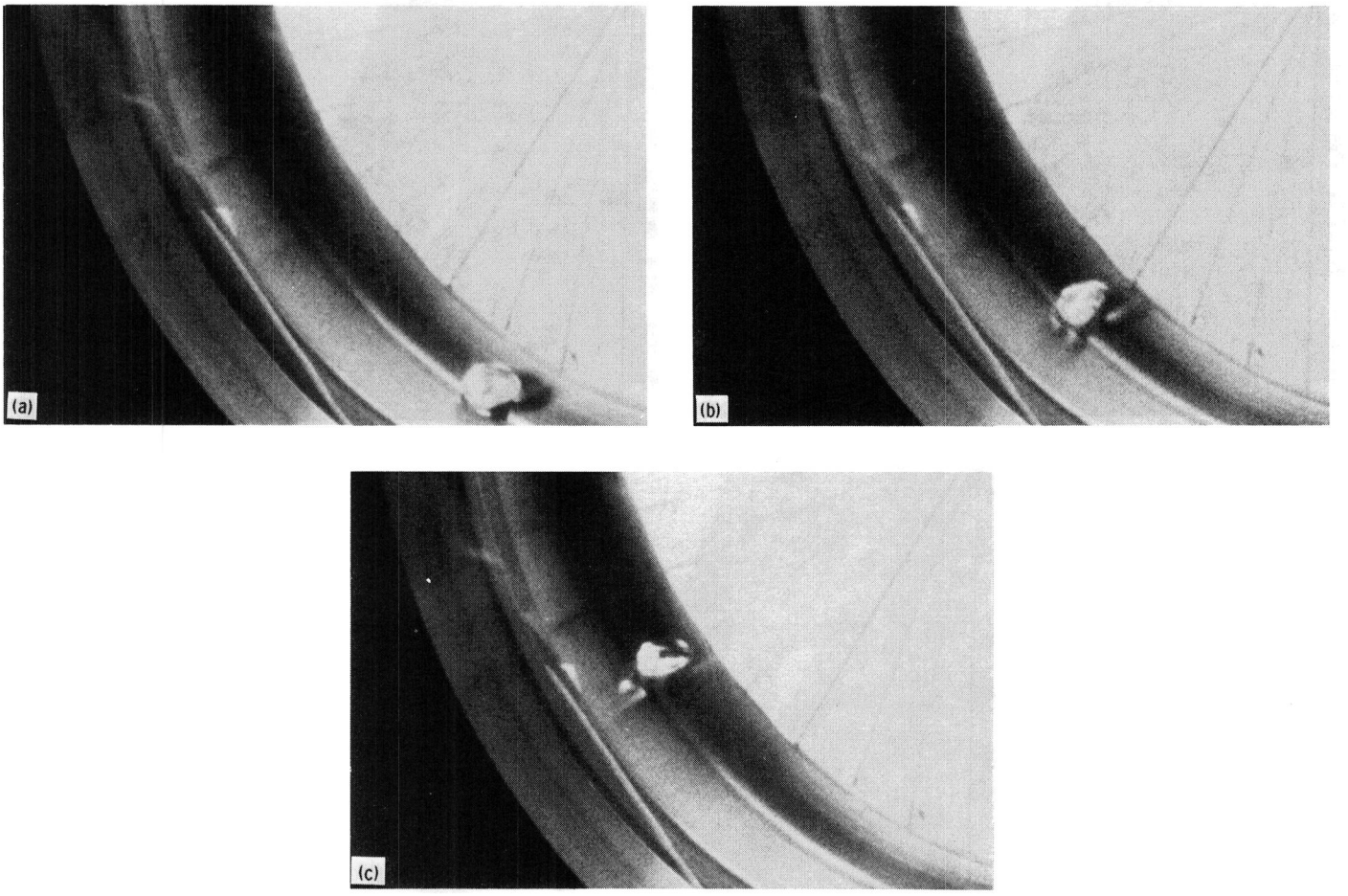


(a) $V = 5.30$ m/s; $We_D = 3.0$; $Re_D = 1400$.
(b) $V = 7.54$ m/s; $We_D = 6.1$; $Re_D = 2000$.
(c) $V = 9.78$ m/s; $We_D = 10.0$; $Re_D = 2600$.

Figure 7.—Four-ring polyphenyl ether (MCS 210) droplet of 1.98-mm radius in air at Bond number of 1.0 and chamber pressure of 98.6 kPa for varying outer-race velocities and Weber and Reynolds numbers (based on diameter).

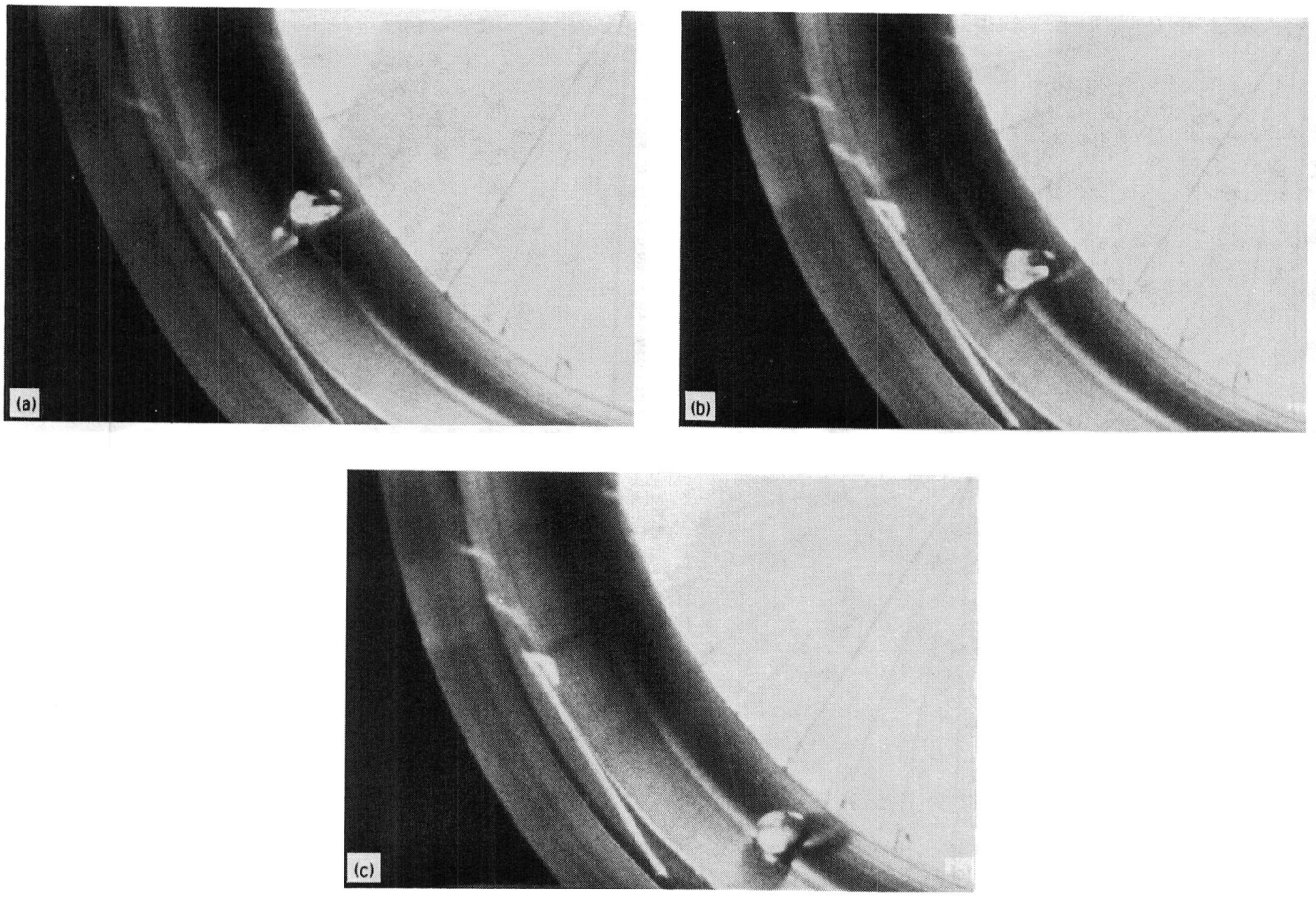


(a) $We_D = 10.0$; $Re_D = 2600$; $P_c = 98.6$ kPa.
(b) $We_D = 7.0$; $Re_D = 1800$; $P_c = 68.9$ kPa.
(c) $We_D = 3.5$; $Re_D = 900$; $P_c = 34.5$ kPa.

Figure 8.—Four-ring polyphenyl ether (MCS 210) droplet of 1.98-mm radius in air at Bond number of 1.0 and outer-race velocity of 9.78 m/s for varying Weber and Reynolds numbers (based on diameter) and chamber pressures.

$$y = C_L x + C_D \tag{10}$$

where

$$y = \frac{8\rho_{oil} g r_d \sin\theta}{3\rho_{air} V^2}$$

$$x = 4\frac{(\eta_{air} V \rho_{oil} g \cos\theta/3)^{1/2}}{\rho_{air} V^2}$$

and

$$\rho_{air} = \frac{\rho_{oil} P_c}{P_{oil}}$$

which yielded $C_L$, $C_D$, and the correlation coefficient by linear regression.

A similar approach with equation (7) yielded $C_L$, $C_D$, and the correlation coefficient for the soft EHL model. The coefficients for the two models for the three fluids and three chamber pressures (table III) suggest that the soft EHL model is superior to the simple HL model. The soft EHL model showed its superiority at droplet sizes and angular positions where the droplet shape deviated substantially from spherical. When the higher angle data were eliminated from consideration in determining the drag and lubrication coefficients from the hydrodynamic equation (10), higher correlations were obtained.

Both models' correlation coefficients improved for low Bond and Weber numbers. These conditions are generally realized for small droplet radii and low chamber pressures (i.e., low air density, table III).

The drag coefficients for the soft EHL model shown in table III and for intermediate radii not included in table III as a function of Reynolds number for all three oils and pressures are shown in figure 9. The range of Reynolds number and uncertainty in the drag coefficient is indicated by the bars. The results were below those of wind tunnel data on smooth spheres. The scatter in the drag coefficient results did not correlate with the variation of fluid type.

The lubrication coefficients for the soft EHL model shown in table III and for intermediate radii not included in table III are shown graphically as a function of Bond number in figure 10 for the three fluids at the three

TABLE III.—COMPARISON OF HYDRODYNAMIC (HL) AND ELASTOHYDRODYNAMIC (EHL) LUBRICATION MODELS FOR THREE FLUIDS AND PRESSURES

| Fluid | Viscosity ratio, $\eta_{oil}/\eta_{air}$ | Chamber pressure, $P_c$ kPa | Droplet radius, $r_d$, mm | Bond number, $B$ | Reynolds number, $Re_D$ | Lubrication coefficient, $C_L$ | | Drag coefficient, $C_D$ | | Correlation coefficient, $R_c$ | |
|---|---|---|---|---|---|---|---|---|---|---|---|
| | | | | | | HL | EHL | HL | EHL | HL | EHL |
| Synthetic paraffin (XRM 109 F-3) | $4.600\times10^{-4}$ | 98.6 | 1.06 | 0.300 | 460-860 | 2.9 | 0.91 | 0.36 | 0.38 | 0.987 | 0.998 |
| | | | 1.75 | .820 | 1135-1900 | 1.8 | .63 | .34 | .34 | .864 | .994 |
| | | 68.9 | 1.06 | .300 | 360-725 | 3.1 | 1.0 | .37 | .38 | .979 | .996 |
| | | | 1.75 | .820 | 930-1530 | 2.0 | .66 | .36 | .35 | .905 | .995 |
| | | 34.5 | 1.06 | .300 | 200-445 | 3.1 | .98 | .44 | .47 | .997 | .999 |
| | | | 1.75 | .820 | 600-800 | 1.7 | .45 | .43 | .45 | .972 | .999 |
| Four-ring polyphenyl ether (MCS 210) | $0.980\times10^{-4}$ | 98.6 | 1.16 | 0.347 | 525-1130 | 3.5 | 1.1 | 0.43 | 0.43 | 0.970 | 0.995 |
| | | | 1.69 | .735 | 1280-2000 | 1.6 | .48 | .39 | .39 | .919 | .998 |
| | | 68.9 | 1.14 | .336 | 430-950 | 3.3 | 1.0 | .39 | .40 | .982 | .997 |
| | | | 1.69 | .735 | 1020-1530 | 1.7 | .47 | .41 | .42 | .993 | 1.000 |
| | | 34.5 | 1.10 | .313 | 180-500 | 3.3 | .96 | .43 | .48 | .997 | 1.000 |
| | | | 1.69 | .735 | 600-770 | 2.5 | .67 | .42 | .44 | .991 | .999 |
| Fluorosilicone (XF 10301) | $0.350\times10^{-4}$ | 98.6 | 1.00 | 0.450 | 490-870 | 2.7 | 0.80 | 0.43 | 0.43 | 0.992 | 0.999 |
| | | | 1.74 | 1.367 | 1130-1980 | .78 | .33 | .44 | .42 | .611 | .993 |
| | | 68.9 | 1.00 | .450 | 380-685 | 2.8 | .83 | .45 | .47 | .997 | 1.000 |
| | | | 1.74 | 1.367 | 925-1590 | 1.2 | .38 | .44 | .44 | .824 | .996 |
| | | 34.5 | 1.00 | .450 | 260-460 | 3.0 | .96 | .49 | .52 | .995 | .999 |
| | | | 1.74 | 1.367 | 630-800 | 1.7 | .46 | .46 | .48 | .996 | .998 |

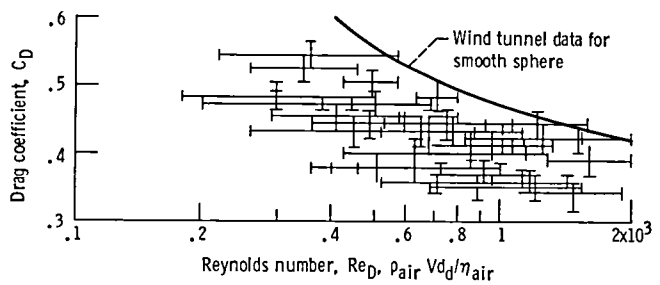


Figure 9.—Drag coefficient as function of Reynolds number (based on diameter) for four-ring polyphenyl ether (MCS 210), fluorosilicone (XF 10301), and synthetic paraffin (XRM 109 F-3) from soft EHL model.

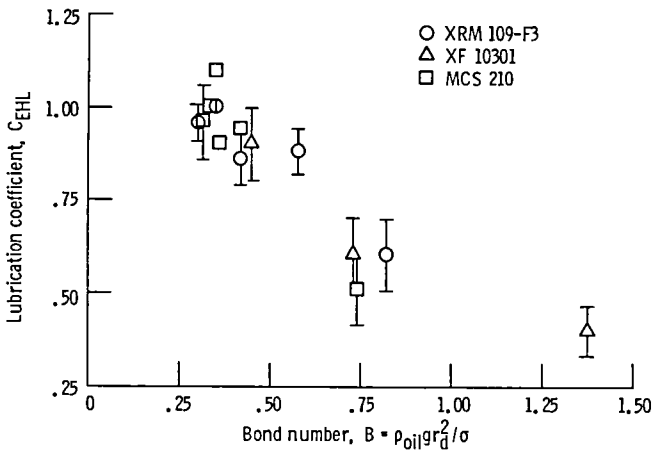


Figure 10.—EHL lubrication coefficient as function of Bond number for four-ring polyphenyl ether (MCS 210), fluorosilicone (XF 10301), and synthetic paraffin (XRM 109 F-3) from soft EHL model.

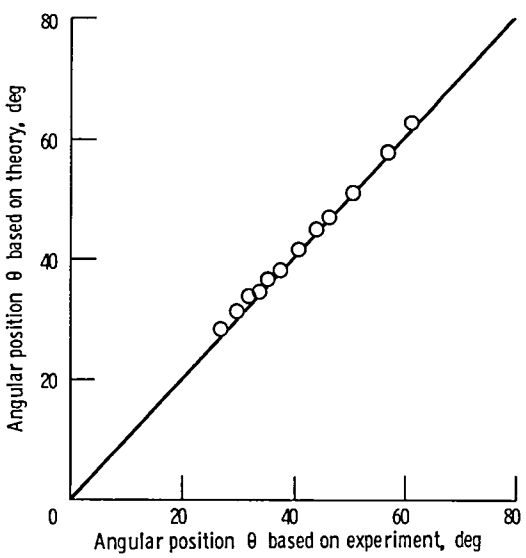


Figure 11.—Angular position predicted by soft EHL model with $C_D = 0.52$ and $C_{EHL} = 0.96$ compared with data on fluorosilicone (MCS 210). Chamber pressure, 34.5 kPa; droplet radius, 1 mm; Bond number, 0.45; Weber number, $1 < We_D < 3.2$; Reynolds number, $250 < Re_D < 450$.

pressures. The data are the average $C_{EHL}$ over the three pressures at a given Bond number. The error bars reflect the uncertainty in the coefficient, the 68 percent probability that another set of measurements of velocity versus $\theta$ of a given radius droplet of known properties for three chamber pressures would produce an average lubrication coefficient $C_{EHL}$ that would fall within the interval shown. Those data points without error bars were taken at one pressure and do not constitute an average.

Figures 11 and 12 indicate the ability of the soft EHL model to predict measurements of angular positions as a function of velocity for a 1-mm-radius droplet of MCS 210 at 34.5-kPa chamber pressure with $C_{EHL}$ of 0.96 and $C_D$ of 0.52. Figure 13 shows the predicted minimum film thickness as a function of $\theta$ from the soft EHL model for the same droplet, chamber pressure, $C_D$, and $C_{EHL}$. Since $h_{min}$ was not measured directly, no data comparison is shown in figure 13.

## Discussion

The semiempirical physical models of a droplet of liquid supported on a gaseous film were corroborated by experimental measurements on three fluids in a rotating outer race in the presence of air at three chamber pressures. The unknown constants resulting from the soft EHL model (a drag coefficient $C_D$ and a lubrication coefficient $C_{EHL}$) were found to have plausible values (0.4 and 1.0, respectively) for those cases where surface tension forces dominated over gravity forces and air inertial forces.

The experimental apparatus was suitable for testing the models as long as the droplets were not at excessively high angles. At high $\theta$ the outer-race velocity was large enough to make the Weber number excessive, and the droplet shape deviated substantially from spherical. The film thickness became large because the radial force became smaller as $\theta$ increased toward 90°, and the outer-race velocity was large enough to drag the droplet up to higher $\theta$. The film Reynolds numbers here were too large to justify the neglect of the inertial terms in the film region. Experimentally the droplets were observed to oscillate in the $y$ direction at angles above 60° and to stand off the race sufficiently to blow axially ($y$ direction) off the race and splatter against the viewing port glass. The nature of the outer-race geometry was such that it constituted a viscous pump, taking air in axially and driving it radially and tangentially out to the outer race and then tangentially and axially over the outer race back out to the chamber. The outer-race radius, $r_{b,y} = -6.55$ mm, was necessary to keep the droplet from being carried out of the outer race axially. At the higher angles the film thickness became large enough to permit the droplet's

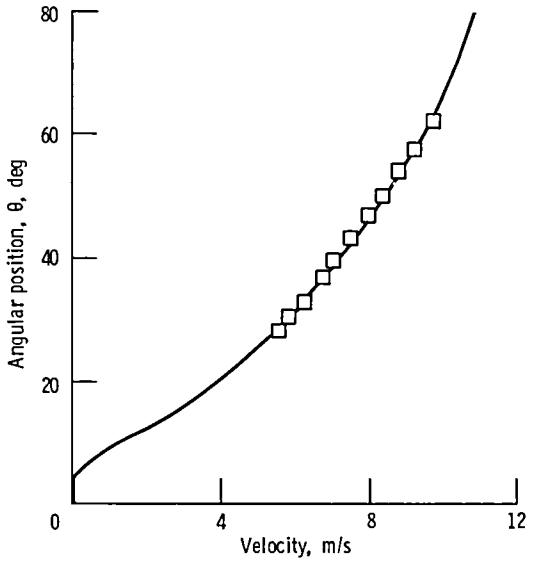


Figure 12.—Angular position as function of outer-race velocity predicted by soft EHL model with $C_D = 0.52$ and $C_{EHL} = 0.96$ compared with data on fluorosilicone (MCS 210). Chamber pressure, 34.5 kPa; droplet radius, 1 mm; Bond number, 0.45; Weber number, $1 < We_D < 3.2$; Reynolds number, $250 < Re_D < 450$.

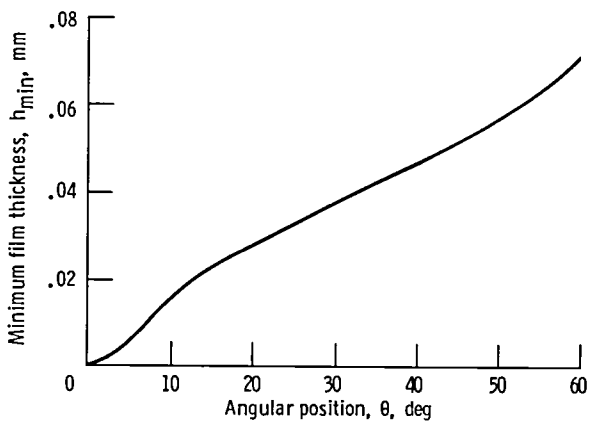


Figure 13.—Minimum film thickness as function of angular position predicted by soft EHL model for $C_D = 0.52$ and $C_{EHL} = 0.96$ for fluorosilicone (MCS 210) chamber pressure, 34.5 kPa; droplet radius, 1 mm; Bond number, 0.45; Weber number, $1 < We_D < 3.2$; Reynolds number, $250 < Re_D < 500$.

escape when combined with the high air velocities driven by the large outer-race velocities.

At the low end of the droplet angle spectrum the outer-race velocity was low as long as the droplet size was not excessive and the minimum thickness was small. This experimental domain was ideal for testing the theoretical models, the Weber numbers were small, and the film skin friction terms were becoming comparable to the air inertial drag terms so that differences in film lubrication models could have an appreciable effect on the results. When the air inertial drag dominated over the film skin friction, the tangential force balance was dominated by the balance of gravity forces and air drag, and the method of determining film thickness and the effect on the skin friction term in the tangential force balance became less significant. Practically it was difficult to keep the droplet at angles below 15° because the film thickness was becoming so small that the rms surface roughness combined with minor vibrations in the outer-race rotations caused asperity contact and the droplet wet the surface.

Both models indicated that the contact area ($\pi r_d^2$ in the HL model and $\eta D_x D_y/4$ in the EHL model) was independent of $\theta$. However, the EHL elliptical contact area was typically 20 percent larger than the HL contact area (i.e., $D_x D_y/4r_d^2 \simeq 1.2$). The droplet was settling into the outer-race geometry more than was visually apparent for the low-Bond-number cases.

No appreciable motion was observed in the oil droplets tested since the ratios of oil viscosity to air viscosity were typically $10^4$. The neglect of these effects in the physical models appeared to be justified for these experimental conditions.

## Conclusions

The dominant physical parameters governing the failure of lubricant droplets to wet nonconformal conjunctions because of a gaseous film between the droplet and the solid surface have been delineated by comparing two film lubrication models with experimental measurements. For sufficiently low Bond numbers $\rho_{oil} g r_d^2/\sigma$ the experimental droplet angular position $\theta$ on a rotating surface correlated well with two dimensionless groups: $\rho_{air} V^2/\rho_{oil} r_d g$ and $\eta_{air} V/\rho_{oil} r_d^2 g$. Two constants were determined from experiment (a drag coefficient $C_D \simeq 0.4$ and a lubrication coefficient $C_L \simeq 3.0$) when using a simple hydrodynamic model. A more complex soft elastohydrodynamic lubrication model correlated $\theta$ with the parameters $\rho_{air} V^2/\rho_{oil} r_d g$, $\eta_{air} V/\rho_{oil} r_d^2 g$, $r_{b,x}/r_d$, and $r_{b,y}/r_d$ for low Bond numbers with a drag coefficient $C_D \simeq 0.4$ and a lubrication coefficient $C_{EHL} \simeq 1.0$. Furthermore the soft EHL model predicted $\theta$ for a wider range of Reynolds and Bond numbers if the model incorporated a drag-coefficient-versus-Reynolds-number relation and a lubrication-coefficient-versus-Bond-number relation.

It has been suggested (Kingsbury, 1969) that, as the air pressure is reduced within the chamber, wetting of the outer race by the droplet occurs because the droplet-outer-race conjunction becomes starved of lubricant (i.e., air). However, lowering the air pressure only served to reduce the density of the air and hence the aerodynamic drag on the droplet in this configuration. The droplet remained fully flooded with lubricant (i.e., surrounded by air whose viscosity remained virtually unchanged). It

is true that as the pressure was reduced, the droplet sank to lower angles because of the reduction in aerodynamic drag. At the lower angles the component of gravity in the radial direction became greater and the film became so thin that asperity contact caused droplet wetting of the outer race. If, however, the velocity of the outer race was progressively increased as the chamber pressure was decreased, the droplet remained at a constant angular position and the film did not become so thin as to allow asperity contact and subsequent wetting of the outer race by the droplet.

Lewis Research Center
National Aeronautics and Space Administration
Cleveland, Ohio, April 5, 1985

## References

1. Hamrock, B.J.; and Dowson, D.: Isothermal Elastohydrodynamic Lubrication of Point Contacts, Part IV—Starvation Results. J. Lubr. Technol., vol. 99, no. 1, Jan. 1977, pp. 15-23.
2. Hamrock, Bernard J.; and Dowson, Duncan: Elastohydrodynamic Lubrication of Elliptical Contacts for Materials of Low Elastic Modulus, I—Fully Flooded Conjunction. J. Lubr. Technol., vol. 100, no. 2, Apr. 1978, pp. 236-245.
3. Hamrock, B.J.; and Brewe, D.: Simplified Solution for Stresses and Deformations. J. Lubr. Technol., vol. 105, no. 2, Apr. 1983, pp. 171-177.
4. Kingsbury, E.P.: Fluid State in EHL Inlet Region. Tribology, vol. 2, Nov. 1969, p. 249.

| 1. Report No. | 2. Government Accession No. | 3. Recipient's Catalog No. |
|---|---|---|
| NASA TP-2500 | | |

| 4. Title and Subtitle | 5. Report Date |
|---|---|
| Mechanics of a Gaseous Film Barrier to Lubricant Wetting of Elastohydrodynamically Lubricated Conjunctions | August 1985 |
| | 6. Performing Organization Code: 505-33-12 |
| 7. Author(s): Joseph M. Prahl and Bernard J. Hamrock | 8. Performing Organization Report No.: E-2523 |
| | 10. Work Unit No. |
| 9. Performing Organization Name and Address: National Aeronautics and Space Administration, Lewis Research Center, Cleveland, Ohio 44135 | 11. Contract or Grant No. |
| | 13. Type of Report and Period Covered: Technical Paper |
| 12. Sponsoring Agency Name and Address: National Aeronautics and Space Administration, Washington, D.C. 20546 | 14. Sponsoring Agency Code |

15. Supplementary Notes

Joseph M. Prahl, Case Western Reserve University, Cleveland, Ohio (work done under NASA grant NCC 3-30); Bernard J. Hamrock, Lewis Research Center. Presented at Eleventh Leeds-Lyon Symposium on Mixed Lubrication and Lubricated Wear, Leeds, England, Sept. 4-7, 1984.

16. Abstract

Two analytical models, one based on simple hydrodynamic lubrication and the other on soft elastohydrodynamic lubrication, are presented and compared to delineate the dominant physical parameters that govern the mechanics of a gaseous film between a small droplet of lubricant and the outer race of a ball bearing. Both models are based on the balance of gravity forces, air drag forces, and air film lubrication forces and incorporate a drag coefficient $C_D$ and a lubrication coefficient $C_L$ to be determined from experiment. The soft elastohydrodynamic lubrication (EHL) model considers the effects of droplet deformation and solid-surface geometry; the simpler hydrodynamic lubrication (HL) model assumes that the droplet remains essentially spherical. The droplet's angular position depended primarily on the ratio of gas inertia to droplet gravity forces and on the gas Reynolds number and weakly on the ratio of droplet gravity forces to surface tension forces (Bond number) and geometric ratios for the soft EHL. An experimental configuration in which an oil droplet is supported by an air film on the rotating outer race of a ball bearing within a pressure-controlled chamber produced measurements of droplet angular position as a function of outer-race velocity droplet size and type, and chamber pressure. For Bond numbers less than 0.5 (large surface tension forces), both models correlated the experimental data with a nearly constant $C_D$ of 0.4 and a $C_L$ of 3.0 for HL or 1.0 for soft EHL. For larger variations in Bond number B and Reynolds number $Re_D$, the soft EHL model showed superior correlation of the experimental data with experimentally determined $C_D$ versus $Re_D$ and $C_L$ versus B.

| 17. Key Words (Suggested by Author(s)) | 18. Distribution Statement |
|---|---|
| Droplet kinematics<br>Elastohydrodynamic lubrication<br>Ball bearings<br>Lubricant wetting | Unclassified - unlimited<br>STAR Category 37 |

| 19. Security Classif. (of this report) | 20. Security Classif. (of this page) | 21. No. of pages | 22. Price* |
|---|---|---|---|
| Unclassified | Unclassified | 16 | A02 |

*For sale by the National Technical Information Service, Springfield, Virginia 22161

NASA-Langley, 1985

National Aeronautics and
Space Administration

Washington, D.C.
20546



**BULK RATE**
**POSTAGE & FEES PAID**
NASA Washington, DC
Permit No. G-27